Original Article | Breast Imaging

eISSN 2005-8330
https://doi.org/10.3348/kjr.2020.0760
Korean J Radiol 2021;22(7):1021-1033

Korean Journal of Radiology
KJR

Dynamic Contrast Enhanced MRI and Intravoxel Incoherent Motion to Identify Molecular Subtypes of Breast Cancer with Different Vascular Normalization Gene Expression

Wan-Chen Tsai[1, 2], Kai-Ming Chang[3], Kuo-Jang Kao[3]

Departments of [1]Radiology and [3]Research, Koo Foundation Sun Yat-Sen Cancer Center, Taipei, Taiwan; [2]School of Medicine, National Yang-Ming Chiao-Tung University, Taipei, Taiwan

Objective: To assess the expression of vascular normalization genes in different molecular subtypes of breast cancer and to determine whether molecular subtypes with a higher vascular normalization gene expression can be identified using dynamic contrast-enhanced (DCE) magnetic resonance imaging (MRI) and intravoxel incoherent motion (IVIM) diffusion-weighted imaging (DWI).

Materials and Methods: This prospective study evaluated 306 female (mean age ± standard deviation, 50 ± 10 years), recruited between January 2014 and August 2017, who had *de novo* breast cancer larger than 1 cm in diameter (308 tumors). DCE MRI followed by IVIM DWI studies using 11 different b-values (0 to 1200 s/mm^2) were performed on a 1.5T MRI system. The Tofts model and segmented biexponential IVIM analysis were used. For each tumor, the molecular subtype (according to six [I-VI] subtypes and PAM50 subtypes), expression profile of genes for vascular normalization, pericytes, and normal vascular signatures were determined using freshly frozen tissue. Statistical associations between imaging parameters and molecular subtypes were examined using logistic regression or linear regression with a significance level of $p = 0.05$.

Results: Breast cancer subtypes III and VI and PAM50 subtypes luminal A and normal-like exhibited a higher expression of genes for vascular normalization, pericyte markers, and normal vessel function signature ($p < 0.001$ for all) compared to other subtypes. Subtypes III and VI and PAM50 subtypes luminal A and normal-like, versus the remaining subtypes, showed significant associations with K^{trans}, k_{ep}, v_p, and $IAUGC_{BN}90$ on DEC MRI, with relatively smaller values in the former. The subtype grouping was significantly associated with D, with relatively less restricted diffusion in subtypes III and VI and PAM50 subtypes luminal A and normal-like.

Conclusion: DCE MRI and IVIM parameters may identify molecular subtypes of breast cancers with a different vascular normalization gene expression.

Keywords: *Breast cancer; Vascular normalization; Molecular subtype; DCE MRI; IVIM*

INTRODUCTION

Therapeutic targeting of angiogenic pathways is promising, because it inhibits the pathways that play a key role in tumor growth and progression [1,2]. Unlike normal blood vessels, tumor vessels often show architectural and functional abnormalities, such as tortuosity, leakiness, and loss of pericytes [3-5]. Poor pericyte presence and function

Received: June 11, 2020 **Revised:** February 1, 2021 **Accepted:** February 4, 2021
This study is supported by the Taiwan Ministry of Health and Welfare, Surcharge of Tobacco Products (no. MOHW103-TD-B-111-11, MOHW104-TDU-B-212-124-007, MOHW105-TDU-B-212-134004, MOHW106-TDU-B-212-144004) (CCGII Program).
Corresponding author: Wan-Chen Tsai, MD, Department of Radiology, Koo Foundation Sun Yat-Sen Cancer Center, 125 Lider Rd, Pei-Tou district, Taipei 112, Taiwan.
• E-mail: wctsai@kfsyscc.org

may contribute to the disruption of endothelial lining, leading to vascular leakiness and dissemination of tumor cells [5-8]. Anti-angiogenesis treatment at an appropriately low dose is associated with vascular normalization by pruning and remodeling of abnormal tumor vessels. Normalized tumor vasculature and function means reduced tumor hypoxia and interstitial fluid pressure and improved blood perfusion, resulting in better efficacy of various therapies [1,9]. Breast cancer is a heterogeneous disease and consists of different molecular subtypes [10-13] with different angiogenetic characteristics and expressions of genes that regulate vascular normalization [14-16]. The subtypes with lower vascular normalization genes may have more abnormal tumor vessels, which may benefit from the vascular normalization effect of anti-angiogenesis treatment more than subtypes with higher vascular normalization genes can [1,9].

Bevacizumab was the first anti-angiogenic drug approved for the treatment of cancer. After the positive results from the E2100 randomized phase III trial, the United States Food and Drug Administration granted accelerated approval for bevacizumab combined with weekly paclitaxel for first-line treatment of human epidermal growth factor receptor 2 (HER-2) negative metastatic breast cancer in 2008 [17]. The subsequent randomized phase III trials, AVADO, RIBBON-1, and RIBBON-2, showed improved progression-free survival but no increase in overall survival with the addition of bevacizumab to chemotherapy in patients with HER-2 negative metastatic breast cancer [18-20]. We hypothesized that the clinical benefit of anti-angiogenesis treatment combined with chemotherapeutic regimens is unclear because the difference in vascular normalization genes among breast cancer molecular subtypes has been overlooked.

A previous study categorized 327 breast cancers into six different molecular subtypes (I-VI) using the expression of 783 genes (GSE20685 cohort) [13]. This study showed a strong correlation between these six molecular subtypes and the intrinsic subtypes of PAM50 (luminal A, luminal B, HER-2, basal, and normal-like) with some significant differences [13,21]. For instance, subtype I breast cancer resembles the basal-like intrinsic subtype [13]. Subtype III is non-basal like triple negative, which does not correspond to a specific PAM50 intrinsic subtype. Subtype IV is genetically similar to the high-risk luminal B subtype, and both subtypes V and VI are luminal A-like. However, subtype V is associated with better long-term survival and appears to be less sensitive to chemotherapy than subtype VI. Both subtype III (estrogen receptor [ER] low to negative) and subtype VI (ER-positive) breast cancer share the same high expression of vascular normalization signature genes [13].

In this prospective study, we first assessed the expression of vascular normalization gene expression in different molecular subtypes of breast cancer according to types I to VI [13] and PAM50 [21]. Then, we aimed to determine whether the subtypes with a higher vascular normalization gene expression could be identified with parameters of dynamic contrast-enhanced (DCE) magnetic resonance imaging (MRI) and intravoxel incoherent motion (IVIM) diffusion-weighted imaging (DWI).

MATERIALS AND METHODS

This prospective study was approved by the Institutional Review Board (IRB No. 20131018A). Written informed consent was obtained from all participants. From January 2014 to August 2017, 329 consecutive, eligible female with core needle biopsy-proven invasive ductal carcinoma larger than 1 cm on ultrasound (US) imaging were recruited. Figure 1 shows an overview of the characteristics of the female included in the study, as well as those excluded. The exclusion criteria were: failed breast MRI exam or insufficient tissue collection for cancer molecular subtyping (n = 23). A total of 306 female with 308 tumors were enrolled in the study. Breast MRI examinations were performed between the 5th and 15th days of each participant's menstrual cycle. Representative frozen tumor tissues were collected for gene expression profiling either from surgically removed breast tumors or from US-guided biopsy sample cores using a 14-gauge biopsy gun (Bard Max Core).

DCE MRI and IVIM Acquisition

Breast MRI examinations were performed with the participant in the prone position, using a 1.5T imaging unit (Optima MR450 W; GE Healthcare). The scanning protocol of DCE MRI with B1 mapping and T1 mapping was the same as previously described [22]. For DCE MRI, intravenous gadobutrol (Gadovist, Bayer Schering) contrast injection was performed at the right antecubital fossa at a dose of 0.1 mmoL/kg and injection rate 3 mL/sec, followed by 20 mL normal saline purge at the same rate. After DCE MRI, IVIM DWI studies were performed, and diffusion gradient encoding was applied in three orthogonal directions with 11 b-values (0, 50, 100, 150, 200, 300, 400, 600, 800, 1000,

https://doi.org/10.3348/kjr.2020.0760

Korean Journal of Radiology
KJR

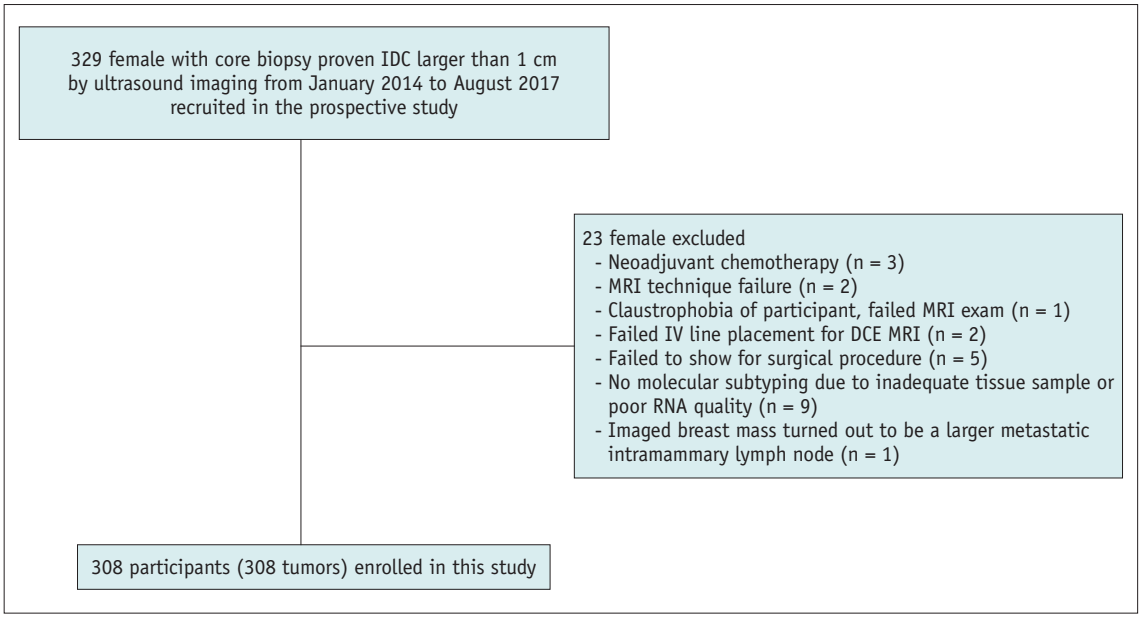

Fig. 1. Flow chart for study participant selection. DCE = dynamic contrast enhanced, IDC = invasive ductal carcinoma, IV = intravenous, MRI = magnetic resonance imaging

and 1200 s/mm^2, Supplementary Materials 1).

MRI Data Analysis (Supplementary Materials 1)

Imaging analysis was performed using the MIStar 3.2 software (Apollo Medical Imaging Technology) with calculations of pharmacokinetic parameters based on the two-compartment Tofts model [23] and IVIM analysis [24].

Tofts Model Analysis

The method for obtaining pharmacokinetic parameters in DCE MRI using the Tofts model has been previously described [22,23]. Two sets of tumor T1 values were used for the Tofts model analysis. We used a fixed T1 value of 1650 ms for all female (n = 306), since the first 80 female did not have a B1 map scan. For female with B1 map scans (n = 236), we also used the B1 corrected T1 value of the tumor to convert signal intensity to concentration vs. time curve. The pharmacokinetic parameters K^{trans}, k_{ep} ($k_{ep} = K^{trans}/v_e$,), v_e, v_p, and $IAUGC_{BN}90$ were computed.

IVIM Analysis

IVIM data was analyzed using a segmented bi-exponential fitting equation [24]. Maps of the IVIM parameters, including D, D_p, and f, were automatically calculated. The tumor region of interest (ROI) was manually defined with growth by threshold function by a breast radiologist (with 9 years of experience in breast MRI) independently blinded to genetic results within a week after the MRI study at the maximal tumor cross-sectional area at phase 32 of the enhancing tumor [25] and in an axial slice with the largest tumor area on DWI at b = 1000 sec/mm^2.

Gene Expression Profiling

Gene expression profiling was performed on freshly frozen tumor specimens obtained by surgical resection (n = 243) or biopsy (n = 65) as described previously [13]. Total RNA was extracted using TRIzol (ThermoFisher Scientific) and further purified using the RNeasy Mini Kit (Qiagen). The quality of the extracted RNA was assessed using an RNA 6000 Nano Kit in an Agilent 2100 Bioanalyzer (Agilent Technologies). The RNA samples used had an average RNA integrity number of 8.6 ± 0.7 (mean ± standard deviation). Hybridization targets were prepared from total RNA using the Affymetrix GeneChip 3'IVT plus reagent kit and hybridized to U133 plus 2.0 arrays (Affymetrix). The expression intensity of each gene was scaled to a trimmed mean of 500 using the MAS5.0 software, transformed to a base-2 logarithm, and quantile-normalized to a reference standard cohort (GSE20685) established in the laboratory [13].

The hormone receptor status was determined by mRNA expression (Table 1). The molecular subtype of each tumor (six subtypes and PAM50 subtypes) was determined as described previously [13,21]. The expression levels of five vascular normalization genes (*CDH5*, *TIE1*, *EPAS1*, *KDR*, and *FLT4*) [6,26], six pericyte marker genes (*ACTA2*, *ANGPT1*, *CSPG4*, *LAMB1*, *PDGFRB*, and *RGS5*) [7], and four

 https://doi.org/10.3348/kjr.2020.0760

Table 1. The Characteristics of Subjects in the Study MRI Cohort vs. the Previous GSE20685 Cohort

Characteristics	Study MRI Cohort (n = 308 Tumors for Six Molecular Subtype and PAM50 Subtypes; Otherwise, n = 306 Patients)*	Previous GSE20685 Cohort (n = 327)†	*P*
Age, years, mean ± SD	50 ± 10	48 ± 11	0.276
Initial stage			0.001
I	69 (22.5)	69 (21.1)	
II	179 (58.5)	147 (45.0)	
III	55 (18.0)	103 (31.5)	
IV	3 (1.0)	8 (2.4)	
Tumor stage			< 0.001
T1	96 (31.4)	101 (30.9)	
T2	202 (66.0)	188 (57.5)	
T3	8 (2.6)	26 (8.0)	
T4	0 (0)	12 (3.7)	
Nodal stage			0.014
N0	149 (48.7)	137 (41.9)	
N1	100 (32.7)	87 (26.6)	
N2	38 (12.4)	63 (19.3)	
N3	19 (6.2)	40 (12.2)	
Receptor status‡			
ER+	204 (66)	204 (62.4)	0.489
HER-2+	58 (19)	75 (22.9)	0.489
PR+	250 (81)	258 (78.9)	0.489
Six molecular subtype§			0.489
I	41 (13.4)	37 (11.3)	
II	32 (10.5)	34 (10.4)	
III	21 (6.9)	41 (12.5)	
IV	84 (27.5)	81 (24.8)	
V	30 (9.8)	41 (12.5)	
VI	100 (32.7)	93 (28.4)	
PAM50 subtypes	Tumor (n = 308)		0.489
Basal	57 (18.5)	54 (16.5)	
HER-2	55 (17.9)	62 (19.0)	
Luminal B	70 (22.7)	72 (22.0)	
Luminal A	105 (34.1)	103 (31.5)	
Normal-like	21 (6.8)	36 (11.0)	

Data are number of subjects with % in parentheses unless specified otherwise. ER: AffyID 205225_at cutoff 11.61956. HER-2: AffyID 216836_s_at cutoff 13.26387. PR: AffyID 208305_at cutoff 4.141207. *There were two female with synchronous tumors; 306 patients and 308 total tumors were assessed in this study, †GSE20685 cohort [13], ‡Receptor status -/+ were determined by the mRNA expression using Affymetrix probeset ID, and their cutoff for -/+, §Molecular subtypes described by Kao et al. [13]. ER = estrogen receptor, HER-2 = human epidermal growth factor receptor 2, MRI = magnetic resonance imaging, PR = progesterone receptor, SD = standard deviation

normal vascular signature genes (*ECSCR*, *AOC3*, *CYYR1*, and *FOXO1*) [15] were also obtained from the microarray data for clustering analyses. One-way clustering was used to generate heatmaps (Supplementary Materials 2).

Statistical Analysis

The differences in clinical and molecular characteristics between the current MRI cohort (n = 308) and the previous GSE20685 cohort (n = 327) [13] using the same Affymeterix gene chip were statistically compared. The associations between the expression level (z-score) of genes in vascular normalization, pericyte marker, normal vessel signatures and the grouping of molecular subtypes, including subtypes III and VI versus the four other subtypes and PAM50 subtypes luminal A and normal-like versus basal, HER-2, and luminal B subtypes, were analyzed using linear regression in order

https://doi.org/10.3348/kjr.2020.0760

Korean Journal of Radiology
KJR

to account for ER, progesterone receptor (PR), and HER-2 status (at mRNA expression level). The concordance of the expression patterns of different gene signatures between the two cohorts was evaluated using Spearman's correlation and permutation tests (with 10000 permutations). Similarly, the binary of multinomial logistic regression (nnet package in R), or linear regression analysis, was used to assess the association between parameters of DCE MRI and IVIM and the molecular subtype grouping of III and VI versus the four other subtypes and PAM50 subtypes luminal A and normal-like versus the other PAM50 subtypes to account for ER, PR, and HER-2 status (at expression level). The *p* values of the variables in the regression models were derived using the Wald test (car package in R). A *p* value (adjusted using Hochberg's method) of < 0.05 indicated significance. To classify subtypes III/VI from the other subtypes, receiver operating characteristic curve analysis was performed. Partial correlation analysis was performed between the vascular normalization gene scores and the MRI parameters while controlling ER, PR, and HER-2 [27]. Data analyses and visualization were performed with the statistical software R v4.0 (R Foundation for Statistical Computing, www.r-project.org).

RESULTS

Characteristics of the Breast Cancer Cohort

We recruited a total of 329 female and excluded 23 female (Fig. 1). Two female with two synchronous tumors were included. Therefore, 308 tumors from 306 female (mean age 50 ± 10 years) in total were included. The interval between the breast MRI examination and breast cancer biopsy or surgery for gene expression analysis was 9 ± 7 days (range, 0–39 days). The mean tumor size of our cohort was 2.7 ± 1.2 cm (range, 1–10 cm).

The age, tumor, regional lymph node, distant metastasis (TNM) stages, hormonal receptor status, and molecular subtypes in our MRI study cohort are summarized and compared with the previous GSE20685 cohort (Table 1) [13]. The two cohorts shared similar distribution of molecular subtypes, age at diagnosis, and statuses of ER, PR, and HER-2, but were different in terms of tumor TNM stage (Table 1). No significant difference was seen in the distribution frequencies of different molecular subtypes between the two cohorts [13]. This finding indicates minimal selection bias in our study. The only significant difference in clinical parameters between the two was lower T and N stages in our present cohort. As reported previously [28], the observed downstaging was likely due to the wider use of mammography screening in the recent era. The patient/tumor characteristics of subtypes III/VI versus others in this MRI cohort were not significantly different in terms of age and TN stages, but differed in ER, PR, HER-2 status, and PAM50 subtype (Table 2).

Breast Cancer Subtypes and Vascular Normalization Gene Signatures

To confirm that breast cancer subtypes III and VI exhibited a higher expression of vascular normalization signature genes within our cohort, we evaluated the expression of these genes using one-way clustering analysis. We found a higher expression in subtypes III and VI in the current cohort ($p < 0.001$) (Fig. 2A). Statistical comparison of heat map concordance between the two cohorts [13] showed a high degree of correlation ($r = 0.956$, $p < 0.001$).

Breast cancer subtypes III and VI of both cohorts exhibited similar increased expression of these pericyte-specific genes compared to other subtypes ($r = 0.918$, $p < 0.001$) (Fig. 2B) [7]. Signature genes in normal blood vessels, as reported by Pepin et al. [15], were used for clustering analysis [13]. The same increased expression of the normal vascular signature genes was again observed in both subtype III and VI breast cancer ($p < 0.001$) (Fig. 2C), along with highly concordant heat map patterns between our cohort and the GSE20685 cohort ($r = 0.934$, $p < 0.001$) (Table 3).

PAM50 subtypes basal, HER-2, and luminal B were highly concordant with subtypes I, II, and IV, respectively. We therefore divided the PAM50 subtypes into basal, HER-2, luminal B versus luminal A, and normal-like to increase the number of cases for statistical power (Supplementary Materials 3, Supplementary Table 1, Supplementary Fig. 1). Vascular normalization, pericytes, and normal vascular gene signatures were significantly higher in luminal A and normal-like in comparison with others (all $p < 0.001$ in both cohorts) (Table 3).

Association between MRI Parameters with Molecular Subtypes

In DCE kinetic curve analysis, there was a more delayed persistent enhancement pattern for III and VI as well as for PAM50 subtypes luminal A and normal-like ($p = 0.001$ and $p = 0.002$ respectively) (Table 4). The longer time to reach the maximal enhancement and less maximal slope of signal

https://doi.org/10.3348/kjr.2020.0760

Table 2. The Characteristics of Patients and Tumors of Molecular Subtype III/VI vs. Others in Study MRI Cohort (n = 306 patients, 308 tumors)

Characteristics	Subtype III/VI (n = 121 Tumors for PAM50 Subtypes; Otherwise, n = 120 Patients)	Others (n = 187 Tumors for PAM50 Subtypes; Otherwise, n = 186 Patients)	*P*
Age, years, mean ± SD	50 ± 9	49 ± 11	0.593
Initial stage			0.593
I	28 (23.3)	41 (22.0)	
II	68 (56.7)	111 (59.7)	
III	24 (20.0)	31 (16.7)	
IV	0 (0)	3 (1.6)	
Tumor stage			0.593
T1	40 (33.3)	56 (30.1)	
T2	76 (63.3)	126 (67.7)	
T3	4 (3.3)	4 (2.2)	
T4	0 (0)	0 (0)	
Nodal stage			0.118
N0	48 (40.0)	101 (54.3)	
N1	49 (40.8)	51 (27.4)	
N2	13 (10.8)	25 (13.4)	
N3	10 (8.3)	9 (4.8)	
Receptor status			
ER	95 (79.2)	107 (57.5)	< 0.001
HER-2	10 (8.3)	48 (25.8)	< 0.001
PR	107 (89.2)	141 (75.8)	0.021
PAM50-like subtype			< 0.001
Basal	9 (7.4)	48 (25.7)	
HER-2	7 (5.8)	48 (25.7)	
LumA	72 (59.5)	33 (17.6)	
LumB	13 (10.7)	57 (30.5)	
Normal	20 (16.5)	1 (0.5)	

Data are number of subjects with % in parentheses unless specified otherwise. ER = estrogen receptor, HER-2 = human epidermal growth factor receptor 2, MRI = magnetic resonance imaging, PR = progesterone receptor, SD = standard deviation

increase was significant for subtypes III and VI (both $p < 0.001$) and for PAM50 subtypes luminal A and normal-like ($p < 0.001$ and $p = 0.064$, respectively) (Table 4). These results collectively suggest slower blood flow and lower blood volume or vascular density.

Using the Tofts model for DCE analysis with fixed T1 values, we found a difference in the perfusion-related parameters K^{trans}, k_{ep}, v_p, and $IAUGC_{BN}90$ between subtypes III and VI and other breast cancer subtypes ($p = 0.032$, $p < 0.001$, $p < 0.001$, and $p = 0.010$, respectively) (top of Table 5). All these parameters were lower in subtypes III and VI. In contrast, extravascular-extracellular space (v_e, $p = 0.043$) based on a fixed T1 value was higher for subtypes III and VI. Similar findings were seen in female where T1 values could be B1 corrected, except that differences in K^{trans} and $IAUGC_{BN}90$ were no longer significant based on T1 data after B1 correction (n = 236) (bottom of Table 5). Examples of representative DCE MRI and pharmacokinetic maps of subtype VI and subtype IV breast cancer are shown in Figures 3 and 4. The same direction of difference in the DCE parameters was noted in luminal A and normal-like versus others using the PAM50 subtype. Luminal A and normal-like also showed lower K^{trans}, k_{ep}, v_p, and $IAUGC_{BN}90$ ($p = 0.036$, $p < 0.001$, $p = 0.008$, and $p = 0.022$, respectively) (top of Table 5).

Less restricted diffusion (higher D), and lower S0 (theoretical signal intensity for b-value of 0 sec/mm^2, original signal without diffusion) were found when molecular subtypes III and VI were compared with the combination of other subtypes ($p = 0.006$, $p < 0.001$, respectively) (Table 6). The corresponding maps of IVIM parameters of the same subtype VI and subtype IV breast

https://doi.org/10.3348/kjr.2020.0760

Korean Journal of Radiology
KJR

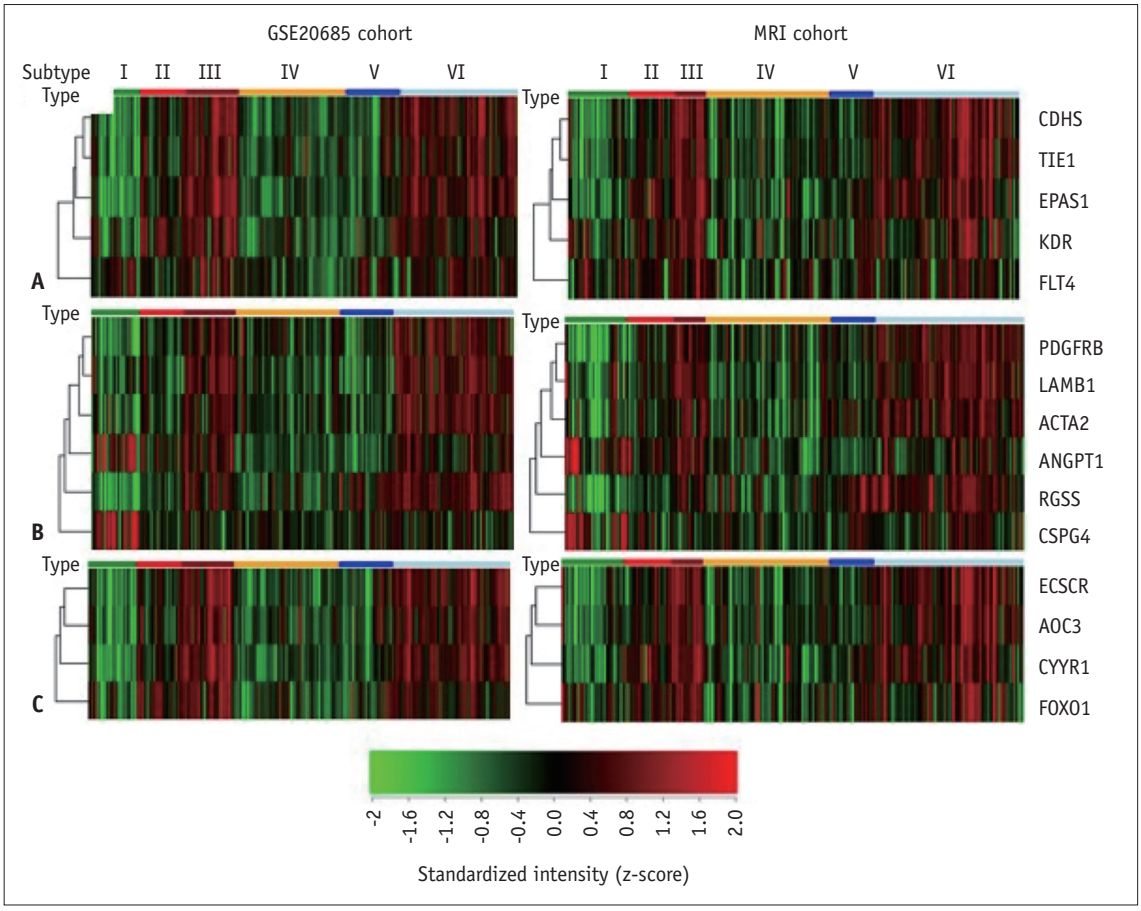

Fig. 2. Comparison of differential expressions of various vascular signatures among breast cancer molecular subtypes between the GSE20685 cohort and the present MRI cohort.

A-C. One-way hierarchical clustering analysis was performed on 327 samples from the GSE20685 cohort and 308 samples from the MRI cohort using genes of **(A)** vascular normalization signature, **(B)** pericyte markers, and **(C)** normal vascular signatures. Genes in the heatmaps of the two cohorts were arranged according to the corresponding dendrograms. The heatmaps depicted the z-scored (across samples) intensities of genes of samples, the brightest green reflects z-scored intensity ≤ -2, the brightest red indicates z-scored intensity ≥ 2, and black represents z-score intensity = 0. Samples (columns) were ordered according to molecular subtype, and genes (rows) were ordered according to the dendrograms of hierarchical clustering results (distance metric is one minus cosine correlation and the linkage function: average linkage) on the z-scored (across samples) gene intensity of data sets. The results showed increased gene expression of all three signatures in subtypes III and VI breast cancer in both cohorts. MRI = magnetic resonance imaging

cancer are shown in Figures 5 and 6. D was also higher in PAM50 subtypes luminal A and normal-like, compared to others (p = 0.031) (Table 6).

Vascular normalization gene expression was significantly higher in subtype III than subtype I, while it was higher in VI than V. The differential DCE MRI and IVIM parameter directions were the same as in the large group analysis (Supplementary Materials 4, Supplementary Tables 2-4).

The optimal cutoff values for these parameters were obtained for differentiation between subtypes III/VI versus others (Supplementary Materials 5, Supplementary Tables 5, 6). The correlation of these vascular normalization gene expressions with the MR perfusion and IVIM parameters is shown in Supplementary Materials 6 (Supplementary Tables 7-9) There is significant correlation between v_e, k_{ep}, D, f, and S0 with these vascular normalization genes. These will be validated in future prospective cohort studies.

DISCUSSION

Our results showed that breast cancers with molecular subtypes III and VI, and PAM50 subtypes luminal A and normal-like, had a higher expression of vascular normalization, pericytes, and normal blood vessel signature genes [13]. Functionally, these subtypes of breast cancer also had MRI measurements associated with more "normal" vascular function. Subtypes III and VI tumors and PAM50 subtypes luminal A and normal-like have less leaky vessels

https://doi.org/10.3348/kjr.2020.0760

Table 3. Vascular Normalization, Pericyte, Normal Vascular Gene Expression Scores of Subtypes III and VI vs. Others; PAM50 Subtypes Luminal A and Normal-Like vs. Basal, HER-2, and Luminal B

Genes	Six Molecular Subtype			PAM50 Molecular Subtype		
	III and VI	Others	*P*	Luminal A and Normal	Basal, HER-2, and Luminal B	*P*
GSE20685 cohort	n = 134	n = 193		n = 139	n = 188	
Vascular Normalization	0.473 ± 0.656	-0.329 ± 0.655	< 0.001	0.255 ± 0.733	-0.188 ± 0.734	< 0.001
Pericyte	0.386 ± 0.514	-0.420 ± 0.593	< 0.001	0.223 ± 0.616	-0.165 ± 0.679	< 0.001
Normal vascular	0.604 ± 0.712	-0.420 ± 0.593	< 0.001	0.309 ± 0.867	-0.228 ± 0.698	< 0.001
Study MRI cohort	n = 121	n = 187		n = 126	n = 182	
Vascular Normalization	0.396 ± 0.702	-0.256 ± 0.686	< 0.001	0.696 ± 0.764	0.233 ± -0.161	< 0.001
Pericyte	0.354 ± 0.495	-0.229 ± 0.668	< 0.001	0.504 ± 0.711	0.256 ± -0.177	< 0.001
Normal vascular	0.582 ± 0.804	-0.377 ± 0.594	< 0.001	0.834 ± 0.742	0.336 ± -0.232	< 0.001

Data are average of z-scored expression of genes in a gene list ± standard deviation. HER-2 = human epidermal growth factor receptor 2, MRI = magnetic resonance imaging

Table 4. Kinetic Curve Analysis of Subtypes III and VI vs. Other Subtypes; PAM50 Subtypes Luminal A and Normal-Like vs. Basal, HER-2, and Luminal B

Parameters	Six Molecular Subtype			PAM50 Molecular Subtype		
	III and VI (n = 121)	Others (n = 187)	*P*	Luminal A and Normal-Like (n = 126)	Basal, HER-2, and Luminal B (n = 182)	*P*
Curve types						
Initial stage			0.691			0.415
Slow	1 (0.8)	0 (0)		1 (0.8)	0 (0)	
Medium	17 (14.0)	23 (12.3)		19 (15.1)	21 (11.5)	
Rapid	103 (85.1)	164 (87.7)		106 (84.1)	161 (88.5)	
Delayed stage			0.001			0.002
Persistent	33 (27.3)	13 (7.0)		32 (25.4)	14 (7.7)	
Plateau	77 (63.6)	133 (71.1)		80 (63.5)	130 (71.4)	
Washout	11 (9.1)	41 (21.9)		14 (11.1)	38 (20.9)	
Curve analysis						
Max enhancement, SI	436 ± 97	444 ± 114	0.934	446 ± 111	437 ± 106	0.801
Max signal to baseline ratio	2.4 ± 0.3	2.4 ± 0.4	0.934	2 ± 0.3	2 ± 0.3	0.801
Final enhancement, SI	733 ± 116	724 ± 121	0.934	748 ± 122	713 ± 114	0.246
Max slope of signal increase, early phase, 1/sec	25 ± 10	31 ± 12	< 0.001	26 ± 12	30 ± 11	0.064
Average slope of signal change, late phase, 1/sec	0.0175 ± 0.2245	-0.0987 ± 0.2087	< 0.001	0.0082 ± 0.2342	-0.0936 ± 0.2034	< 0.001
Time to max enhancement, sec	226 ± 86	183 ± 88	< 0.001	226 ± 85	181 ± 88	< 0.001
Baseline, SI	317 ± 47	315 ± 40	0.934	322 ± 44	311 ± 42	0.341

Data are number for subject with % in parentheses or mean ± standard deviation. HER-2 = human epidermal growth factor receptor 2, SI = signal intensity

(lower K^{trans}, k_{ep}, the volume transfer and rate constant of contrast from extravascular-extracellular space to blood plasma, which measured vascular leakiness and permeability), lower vascular volume (v_p), contain more extravascular-extracellular space (v_e) according to DCE MRI, and have less restricted water diffusion (higher D) on IVIM. These findings could be related to more normal vascular function and reduced need for a higher blood volume to support tumor growth in these subtypes.

In other words, of the two subtyping systems, breast cancer subtypes I, II, IV and PAM50 subtypes basal, HER-2, luminal B with a lower vascular normalization gene expression have more "abnormal" leaky vessels (higher K^{trans}, k_{ep}) and higher vascular volume (higher v_p), lower v_e

https://doi.org/10.3348/kjr.2020.0760

Korean Journal of Radiology
KJR

according to DCE MRI, and have more restricted diffusion (lower D) on IVIM. Breast cancer of these clinically aggressive subtypes with more abnormal leaky vessels (subtypes I, II, and IV; PAM50 subtypes basal, HER-2, and luminal B) may benefit more from the vascular normalization effect of anti-angiogenesis treatment in addition to chemotherapy than those with more normal vessels (subtypes III and VI; PAM50 subtypes luminal A

Table 5. Association between DCE Parameters and the Grouping of Subtypes III and VI vs. Other Subtypes and PAM50 Subtypes Luminal A and Normal-Like vs. Basal, HER-2, Luminal B

Parameters	Six Molecular Subtype			PAM50 Subtype		
	III and VI	Other Subtypes	*P*	Luminal A and Normal	Basal, HER-2, and Luminal B	*P*
Using Fixed T1 value	n = 121	n = 187		n = 126	n = 182	
K^{trans} (1/min/10000)	899 ± 323	1002 ± 398	0.032	916 ± 360	992 ± 380	0.036
k_{ep} (1/min/1000)	427 ± 146	515 ± 164	< 0.001	435 ± 149	511 ± 165	< 0.001
v_e (1/1000)	216 ± 54	200 ± 62	0.043	216 ± 58	199 ± 60	0.094
v_p (1/1000)	10 ± 9	16 ± 10	< 0.001	11 ± 9	16 ± 10	0.008
$iAUGC_{BN}90$ (1/1000)	127 ± 44	145 ± 50	0.010	129 ± 48	144 ± 48	0.022
Using T1 value after B1 correction	n = 88	n = 148		n = 92	n = 144	
K^{trans} (1/min/10000)	1339 ± 481	1299 ± 535	0.936	1348 ± 527	1292 ± 507	0.915
k_{ep} (1/min/1000)	439 ± 159	513 ± 163	0.004	443 ± 155	513 ± 166	0.001
v_e (1/1000)	325 ± 109	265 ± 98	< 0.001	321 ± 101	266 ± 104	< 0.001
v_p (1/1000)	14 ± 14	19 ± 13	0.028	14 ± 13	19 ± 14	0.239
$iAUGC_{BN}90$ (1/1000)	187 ± 68	186 ± 68	0.936	186 ± 69	186 ± 67	0.915

Data are mean ± standard deviation. HER-2 = human epidermal growth factor receptor 2, $IAUGC_{BN}90$ = blood-normalized initial area under the gadolinium concentration curve to 90 s, k_{ep} = rate constant, K^{trans} = volume transfer constant, v_e = volume of EES per unit volume of tissue, v_p = blood plasma volume per unit volume of tissue

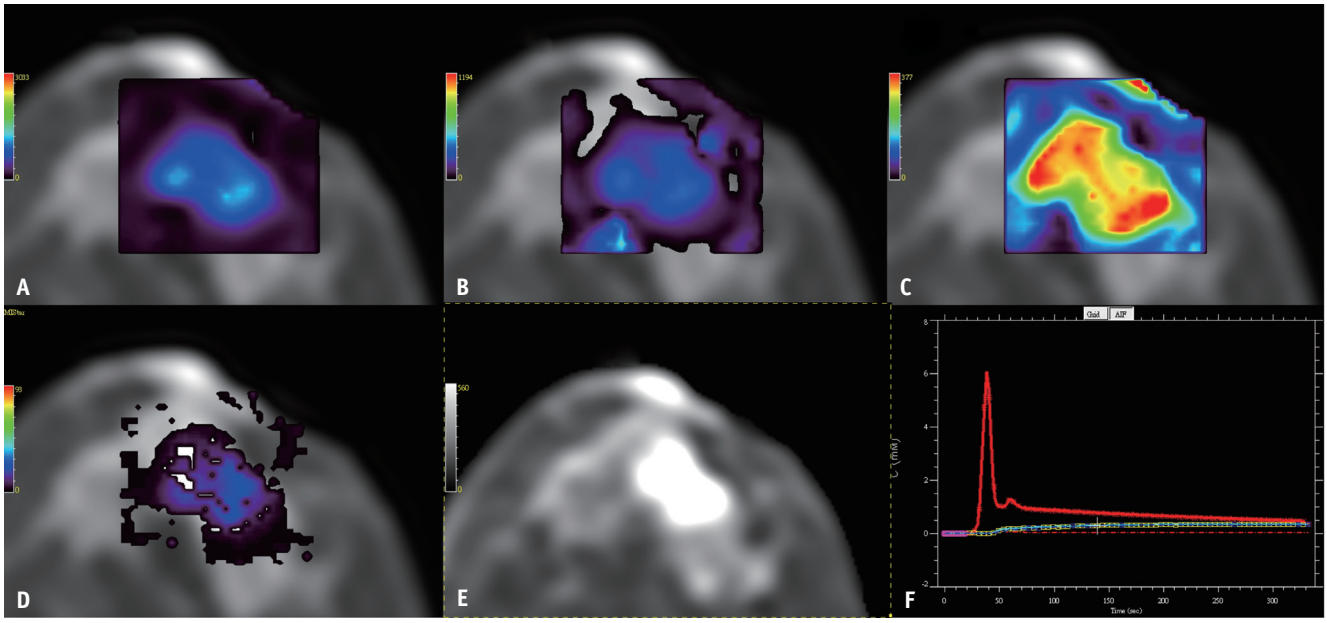

Fig. 3. The representative pharmacokinetic maps of dynamic contrast-enhanced MRI axial slice, fitting curves of Tofts model and model free enhancement signal intensity vs. time curves of a 38-year-old female with molecular subtype VI, luminal A breast cancer.

A-F. The axial pharmacokinetic maps: **(A)** K^{trans}, **(B)** k_{ep}, **(C)** v_e, **(D)** v_p, **(E)** phase 32 of post contrast enhanced T1 weighted fat-saturated MRI (repetition time/echo time = 3.8/1.2 ms; flip angle = 12°; bandwidth = 41.67 kHz; field-of-view = 34 x 34 cm; matrix size = 96 x 80; slice thickness = 3 mm), **(F)** fitted concentration vs. time curves in pharmacokinetic model (red solid line: arterial input function, yellow line: measured concentration within region of interest, red dashed line: perfusion, blue dashed line: leakage). k_{ep} = rate constant, K^{trans} = volume transfer constant, MRI = magnetic resonance imaging, v_e = volume of EES per unit volume of tissue, v_p = blood plasma volume per unit volume of tissue

https://doi.org/10.3348/kjr.2020.0760

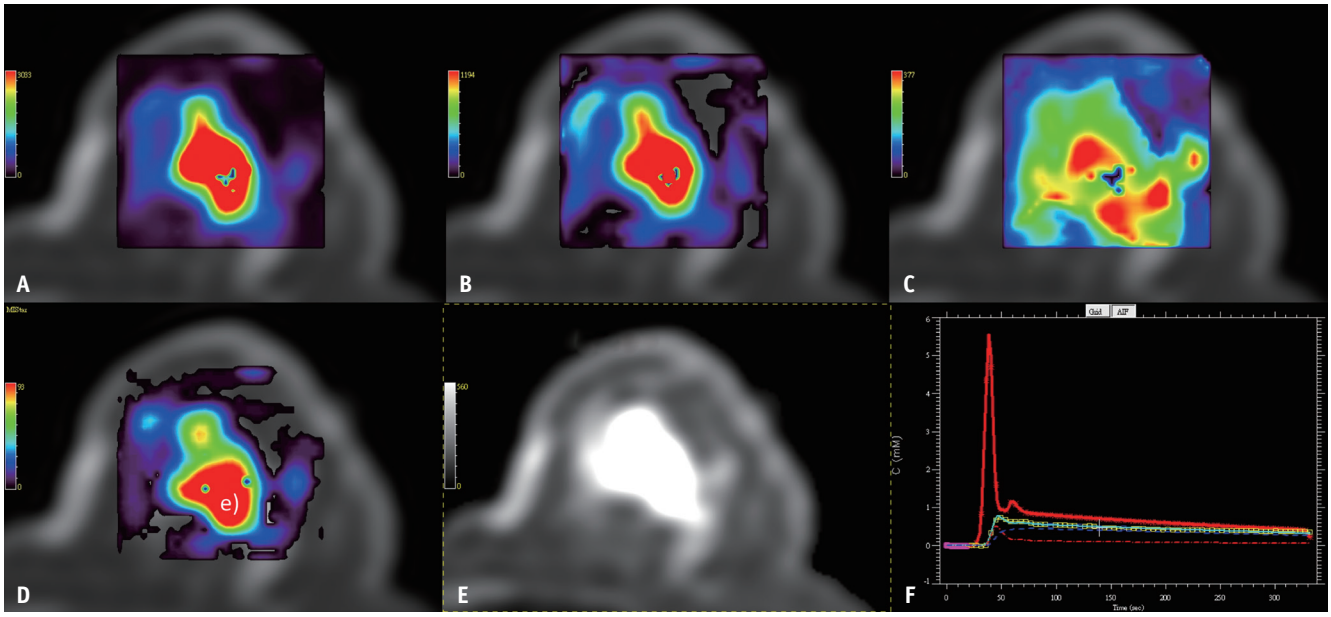

Fig. 4. The representative pharmacokinetic maps of DCE magnetic resonance imaging axial slice, fitting curves of Tofts model and model free enhancement signal intensity vs time curves of a 73-year-old female with molecular subtype IV, luminal B breast cancer using the same scales of the corresponding maps as those in Figure 3.
A-F. Although the maximal enhancement of the whole tumor at the same phase 32 of DCE **(E)** are similar in Figures 3, 4, the **(A)** K^{trans}, **(B)** k_{ep}, **(D)** v_p are lower (blue and purple in color) in subtype VI (Fig. 3) as compared with subtype IV (Fig. 4). The extravascular-extracellular space (v_e) **(C)** is higher in subtype VI (Fig. 3) compared to subtype IV (Fig. 4). The enhancement concentration vs. time kinetic curve (yellow line in **(F)**) shows slow initial and delayed persistent enhancement curve in subtype VI (Fig. 3); while early initial and delayed washout enhancement curve in subtype IV (Fig. 4). DCE = dynamic contrast-enhanced, k_{ep} = rate constant, K^{trans} = volume transfer constant, v_e = volume of EES per unit volume of tissue, v_p = blood plasma volume per unit volume of tissue

Table 6. Association between Intravoxel Incoherent Motion Parameters and the Grouping of Subtype III and VI vs. Others and PAM50 Subtypes Luminal A and Normal-Like vs. Basal, HER-2, and Luminal B

Parameters	Six Molecular Subtype			PAM50 Subtype		
	III and VI (n = 114)	Others (n = 182)	*P*	Luminal A and Normal-Like (n = 119)	Basal, HER-2, and Luminal B (n = 177)	*P*
D, x 10^{-6} mm^2/sec	866 ± 144	829 ± 163	0.006	853 ± 153	837 ± 160	0.031
D_p, x 10^{-5} mm^2/sec	948 ± 166	1003 ± 161	0.067	946 ± 164	1007 ± 161	0.222
f (1/1000)	119 ± 28	118 ± 26	0.448	118 ± 30	119 ± 24	0.790
S0	412 ± 101	486 ± 114	< 0.001	421 ± 107	482 ± 114	0.097

Data are mean ± standard deviation. D = molecular diffusion coefficient of water in tissues, in x 10^{-6} mm^2/s; D_p = pseudodiffusion coefficient associated with blood flow velocity, in x 10^{-5} mm^2/s, f = flowing blood fraction within the tissue volume, in 1/1000, S0 = theoretical signal intensity for b-value of 0 sec/mm^2, and original signal without diffusion.

and normal-like) [1,9]. Furthermore, triple negative breast cancer could be further categorized into basal subtype (I) and non-basal subtype (III) with a differential vascular normalization gene expression based on the DCE MRI and IVIM parameters in our study [13]. Molecular subtype I (basal) with more abnormal vessels may benefit more than subtype III (non-basal triple negative) from the addition of anti-angiogenesis drugs, which facilitate chemotherapy response.

The IVIM parameters of subtypes III and VI and PAM50 subtypes luminal A and normal-like had higher D. Again, less restricted diffusion (higher water diffusion coefficient), possibly reflected larger extravascular-extracellular space (v_e). The lower S0 may indicate lower T2 weighted signal intensity, suggesting less edema or necrosis in subtypes III and VI. Thus, the DCE and IVIM MRI results are consistent with the molecular signature of better functioning, more normalized vasculature in subtypes III and VI, and PAM50 subtypes luminal A and normal-like breast cancer.

To address the issue of B1 inhomogeneity in MR measurements, we used T1 values after B1 correction. As reported previously, B1 inhomogeneity should be considered

https://doi.org/10.3348/kjr.2020.0760

Korean Journal of Radiology
KJR

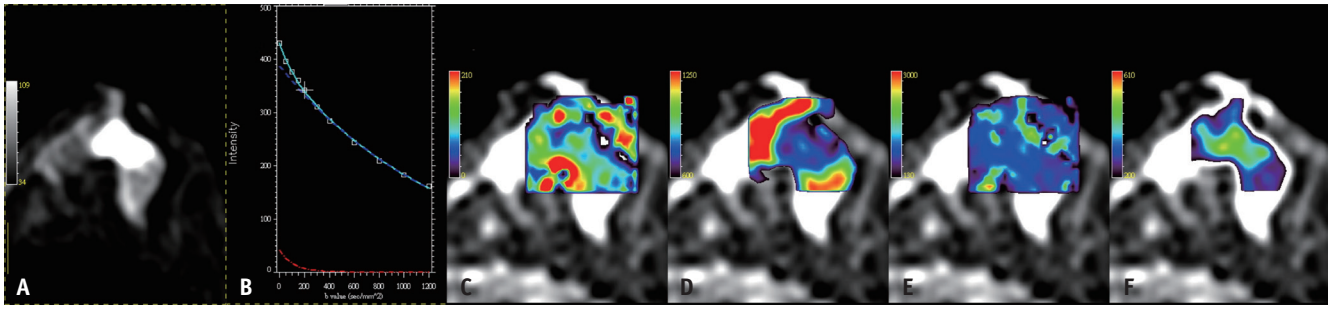

Fig. 5. The representative DWI images, fitting curves, maps of IVIM parameters for a 38-year-old female with molecular subtype VI, luminal A breast cancer.

A-F. The **(A)** DWI images with b = 1000 (repetition time/echo time = 8000/65.9 ms; field of view = 34 x 34 cm; matrix size = 98 x 128; slice thickness = 5 mm; slice gap = 0.5 mm; number of excitation = 3), **(B)** fitted signal intensity vs. b-values curves of IVIM model (red dashed line: pseudo-diffusion, blue dashed line: diffusion, light blue solid line: the signal intensity vs. b-values line), **(C)** f (flowing blood fraction within the tissue volume, in 1/1000), **(D)** D (molecular diffusion coefficient of water in tissues, in x 10^{-6} mm^2/s), **(E)** D_p (pseudo-diffusion coefficient associated with blood flow velocity, in x 10^{-5} mm^2/s), **(F)** S0 (theoretical signal intensity for b-values of 0 sec/mm^2, original signal without diffusion). The tumor in Figure 5 is the same as in Figure 3. DWI = diffusion-weighted imaging, IVIM = intravoxel incoherent motion

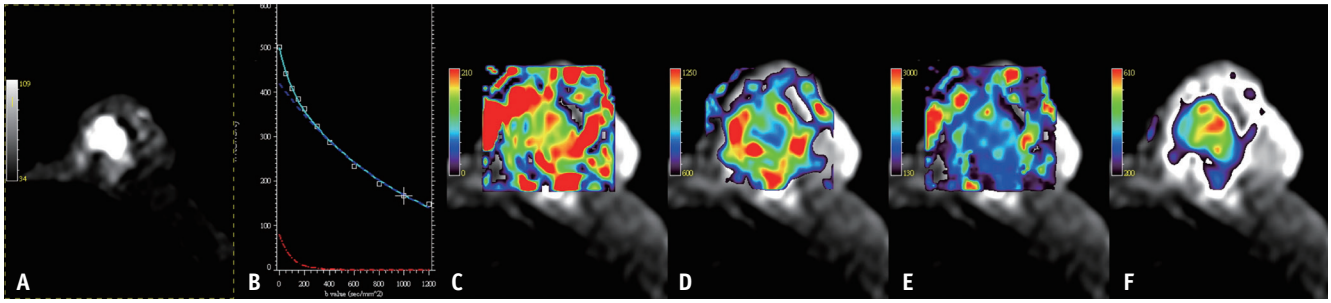

Fig. 6. The representative DWI images, fitting curves, maps of IVIM parameters for a 73-year-old female with molecular subtype IV, luminal B breast cancer.

A-F. The **(A)** DWI images with b = 1000 (repetition time/echo time = 8000/65.9 ms; field-of-view = 34 x 34 cm; matrix size = 98 x 128; slice thickness = 5 mm; slice gap = 0.5 mm; number of excitation = 3), **(B)** fitted signal intensity vs. b-values curves of IVIM model (red dashed line: pseudo-diffusion, blue dashed line: diffusion, light blue solid line: the signal intensity vs. b-values line), **(C)** f (flowing blood fraction within the tissue volume, in 1/1000), **(D)** D (molecular diffusion coefficient of water in tissues, in x 10^{-6} mm^2/s), **(E)** D_p (pseudo-diffusion coefficient associated with blood flow velocity, in x 10^{-5} mm^2/s), **(F)** S0 (theoretical signal intensity for b value of 0 sec/mm^2, original signal without diffusion, in 1/1000). The **(C)** f, **(D)** D, and **(E)** D_p are lower in molecular subtype VI tumor (Fig. 5) compared to molecular subtype IV (Fig. 6). The **(F)** S0 is lower in molecular subtype VI (Fig. 5) compared to molecular subtype IV (Fig. 6). The tumor in Figure 6 is the same as in Figure 4. DWI = diffusion-weighted imaging, IVIM = intravoxel incoherent motion

in breast tumor T1 value estimation for breast DCE MRI even at 1.5T [21] to avoid overestimating the error in pharmacokinetic parameters in tumors on the left side. We also adopted constant T1 values for conversion of signal intensity into tissue concentration vs. time curve for all tumors and compared them to B1 corrected T1 values of tumors used to assess differences in the pharmacokinetic parameters between the two groups. The same results of lower k_{ep} and v_p, and higher v_e in subtypes III and VI and PAM50 subtypes luminal A and normal-like breast cancer were obtained. Thus, the use of constant T1 values without B1 correction to avoid systematic estimation error stemming from B1 inhomogeneity is also acceptable.

There was one limitation in our study. We selected the maximal area slice of the tumor as the ROI for the MR parameter measurement. This approach was adopted for more representative measurements of the whole tumor. However, the probable presence of intratumor heterogeneity could not be addressed.

In conclusion, this study showed that breast cancers with molecular subtypes III and VI, and PAM50 subtypes luminal A and normal-like, had higher expression levels for vascular normalization signature genes. DCE MRI and IVIM parameters may identify these molecular subtypes of breast cancer. Further investigation on the effect of anti-angiogenesis therapy according to different levels of vascular normalization gene expression and DCE MRI and IVIM imaging biomarker findings across molecular subtypes of breast cancers should be performed in the future.

https://doi.org/10.3348/kjr.2020.0760

Supplement

The Supplement is available with this article at https://doi.org/10.3348/kjr.2020.0760.

Conflicts of Interest

The authors have no potential conflicts of interest to disclose.

Acknowledgments

Special thanks to Leighanne Jamie Chen for her English editing efforts, to Chen-Fang Hung and I-Ting Chen for assistance in data management; to Chien-Yuan Lin PhD. for MRI technique and set up assistance, and to the following members of Surgical Oncology for their care and treatment of patients: Chii-Ming Chen, Tsung-Yen Cheng, Benlong Yu, Tzu-Jung Tsai, Chih-Chun Lee, and Hung-Kuang Wei.

Author Contributions

Conceptualization: Wan-Chen Tsai, Kuo-Jang Kao. Data curation: Wan-Chen Tsai, Kai-Ming Chang. Formal analysis: Kai-Ming Chang. Funding acquisition: Wan-Chen Tsai, Kuo-Jang Kao. Investigation: Wan-Chen Tsai, Kuo-Jang Kao. Methodology: all authors. Project administration: Wan-Chen Tsai, Kuo-Jang Kao. Resources: Wan-Chen Tsai, Kuo-Jang Kao. Software: Wan-Chen Tsai, Kai-Ming Chang. Supervision: Wan-Chen Tsai, Kuo-Jang Kao. Validation: Wan-Chen Tsai, Kai-Ming Chang. Visualization: all authors. Writing—original draft: Wan-Chen Tsai. Writing—review & editing: all authors.

ORCID iDs

Wan-Chen Tsai
https://orcid.org/0000-0001-9757-2950
Kai-Ming Chang
https://orcid.org/0000-0002-1042-1605
Kuo-Jang Kao
https://orcid.org/0000-0001-6501-7987

REFERENCES

1. Jain RK. Normalizing tumor microenvironment to treat cancer: bench to bedside to biomarkers. *J Clin Oncol* 2013;31:2205-2218
2. Ruoslahti E. Specialization of tumour vasculature. *Nat Rev Cancer* 2002;2:83-90
3. Jain RK. The Eugene M. Delivery of molecular and cellular medicine to solid tumors. *Microcirculation* 1997;4:1-23
4. Hashizume H, Baluk P, Morikawa S, McLean JW, Thurston G, Roberge S, et al. Openings between defective endothelial cells explain tumor vessel leakiness. *Am J Pathol* 2000;156:1363-1380
5. Barlow KD, Sanders AM, Soker S, Ergun S, Metheny-Barlow LJ. Pericytes on the tumor vasculature: jekyll or hyde? *Cancer Microenviron* 2013;6:1-17
6. Bautch VL. Endothelial cells form a phalanx to block tumor metastasis. *Cell* 2009;136:810-812
7. Armulik A, Genové G, Betsholtz C. Pericytes: developmental, physiological, and pathological perspectives, problems, and promises. *Dev Cell* 2011;21:193-215
8. Fakhrejahani E, Toi M. Tumor angiogenesis: pericytes and maturation are not to be ignored. *J Oncol* 2012;2012:261750
9. Goel S, Duda DG, Xu L, Munn LL, Boucher Y, Fukumura D, et al. Normalization of the vasculature for treatment of cancer and other diseases. *Physiol Rev* 2011;91:1071-1121
10. Harbeck N, Rody A. Lost in translation? Estrogen receptor status and endocrine responsiveness in breast cancer. *J Clin Oncol* 2012;30:686-689
11. Sørlie T, Perou CM, Tibshirani R, Aas T, Geisler S, Johnsen H, et al. Gene expression patterns of breast carcinomas distinguish tumor subclasses with clinical implications. *Proc Natl Acad Sci U S A* 2001;98:10869-10874
12. Guedj M, Marisa L, de Reynies A, Orsetti B, Schiappa R, Bibeau F, et al. A refined molecular taxonomy of breast cancer. *Oncogene* 2012;31:1196-1206
13. Kao KJ, Chang KM, Hsu HC, Huang AT. Correlation of microarray-based breast cancer molecular subtypes and clinical outcomes: implications for treatment optimization. *BMC Cancer* 2011;11:143
14. Rody A, Karn T, Liedtke C, Pusztai L, Ruckhaeberle E, Hanker L, et al. A clinically relevant gene signature in triple negative and basal-like breast cancer. *Breast Cancer Res* 2011;13:R97
15. Pepin F, Bertos N, Laferrière J, Sadekova S, Souleimanova M, Zhao H, et al. Gene-expression profiling of microdissected breast cancer microvasculature identifies distinct tumor vascular subtypes. *Breast Cancer Res* 2012;14:R120
16. Bhati R, Patterson C, Livasy CA, Fan C, Ketelsen D, Hu Z, et al. Molecular characterization of human breast tumor vascular cells. *Am J Pathol* 2008;172:1381-1390
17. Gray R, Bhattacharya S, Bowden C, Miller K, Comis RL. Independent review of E2100: a phase III trial of bevacizumab plus paclitaxel versus paclitaxel in women with metastatic breast cancer. *J Clin Oncol* 2009;27:4966-4972
18. Miles DW, Chan A, Dirix LY, Cortés J, Pivot X, Tomczak P, et al. Phase III study of bevacizumab plus docetaxel compared with placebo plus docetaxel for the first-line treatment of human epidermal growth factor receptor 2-negative metastatic breast cancer. *J Clin Oncol* 2010;28:3239-3247
19. Robert NJ, Diéras V, Glaspy J, Brufsky AM, Bondarenko I, Lipatov ON, et al. RIBBON-1: randomized, double-blind, placebo-controlled, phase III trial of chemotherapy with

or without bevacizumab for first-line treatment of human epidermal growth factor receptor 2-negative, locally recurrent or metastatic breast cancer. *J Clin Oncol* 2011;29:1252-1260
20. Brufsky AM, Hurvitz S, Perez E, Swamy R, Valero V, O'Neill V, et al. RIBBON-2: a randomized, double-blind, placebo-controlled, phase III trial evaluating the efficacy and safety of bevacizumab in combination with chemotherapy for second-line treatment of human epidermal growth factor receptor 2-negative metastatic breast cancer. *J Clin Oncol* 2011;29:4286-4293
21. Parker JS, Mullins M, Cheang MC, Leung S, Voduc D, Vickery T, et al. Supervised risk predictor of breast cancer based on intrinsic subtypes. *J Clin Oncol* 2009;27:1160-1167
22. Tsai WC, Kao KJ, Chang KM, Hung CF, Yang Q, Lin CE, et al. B1 field correction of T1 estimation should be considered for breast dynamic contrast-enhanced MR imaging even at 1.5 T. *Radiology* 2017;282:55-62
23. Tofts PS, Brix G, Buckley DL, Evelhoch JL, Henderson E, Knopp MV, et al. Estimating kinetic parameters from dynamic contrast-enhanced T(1)-weighted MRI of a diffusable tracer: standardized quantities and symbols. *J Magn Reson Imaging* 1999;10:223-232
24. Le Bihan D, Breton E, Lallemand D, Aubin ML, Vignaud J, Laval-Jeantet M. Separation of diffusion and perfusion in intravoxel incoherent motion MR imaging. *Radiology* 1988;168:497-505
25. RSNA. Profile: DCE-MRI quantification version 1.6 - QIBA Wiki. Yumpu.com Web site. https://www.yumpu.com/en/document/view/19229002/profile-dce-mri-quantificationversion-16-qiba-wiki. Published 2011. Accessed November 1, 2017
26. Mazzone M, Dettori D, de Oliveira RL, Loges S, Schmidt T, Jonckx B, et al. Heterozygous deficiency of PHD2 restores tumor oxygenation and inhibits metastasis via endothelial normalization. *Cell* 2009;136:839-851
27. Kim S. ppcor: an R package for a fast calculation to semi-partial correlation coefficients. *Commun Stat Appl Methods* 2015;22:665-674
28. Verdial FC, Etzioni R, Duggan C, Anderson BO. Demographic changes in breast cancer incidence, stage at diagnosis and age associated with population-based mammographic screening. *J Surg Oncol* 2017;115:517-522

 https://doi.org/10.3348/kjr.2020.0760